Hydrol. Earth Syst. Sci. Discuss., 11, 11905–11943, 2014
www.hydrol-earth-syst-sci-discuss.net/11/11905/2014/
doi:10.5194/hessd-11-11905-2014

Hydrology and Earth System Sciences
Discussions

Impacts of a changing climate on a century of extreme flood regime of northwest Australia

A. Rouillard[1], G. Skrzypek[1], S. Dogramaci[1,2], C. Turney[3], and P. F. Grierson[1]

[1]West Australian Biogeochemistry Centre and Ecosystems Research Group, School of Plant Biology, The University of Western Australia, Crawley, WA 6009, Australia
[2]Rio Tinto Iron Ore, Perth, WA 6000, Australia
[3]Climate Change Research Centre, University of NSW, Sydney, NSW 2052, Australia

Received: 7 October 2014 – Accepted: 9 October 2014 – Published: 24 October 2014

Correspondence to: A. Rouillard (alexandra.rouillard@uwa.edu.au, alexandrarouillard@yahoo.ca)

Published by Copernicus Publications on behalf of the European Geosciences Union.

Abstract

Globally, there has been much recent effort to improve understanding of climate change-related shifts in rainfall patterns, variability and extremes. Comparatively little work have focused on how such shifts might be altering hydrological regimes within arid regional basins, where impacts are expected to be most significant. Here, we sought to identify the main hydroclimatic determinants of the strongly episodic flood regime of a large catchment in the semi-arid, subtropical northwest of Australia and to establish the background of hydrologic variability for the region over the last century. We used a monthly sequence of satellite images to quantify surface water expression on the Fortescue Marsh, the largest water feature of inland northwest Australia, from 1988 to 2012. We used this sequence together with instrumental rainfall data to build a multiple linear model and reconstruct monthly history of floods and droughts since 1912. We found that severe and intense regional rainfall events, as well as the sequence of recharge events both within and between years, determine surface water expression on the floodplain (i.e., total rainfall, number of rain days and carried-over inundated area; $R^2_{adj} = 0.79$; p value < 0.001, $E_{RMSP} = 56\,km^2$). The most severe inundation ($\sim 1000\,km^2$) over the last century was recorded in 2000. The Fortescue Marsh was completely dry for 32 % of all years, for periods of up to four consecutive years. Extremely wet years (seven of the 100 years) caused the Marsh to remain inundated for up to 12 months; only 25 % of years (9 % of all months) had floods of greater than $300\,km^2$. Duration, severity and frequency of inundations between 1999 and 2006 were above average and unprecedented when compared to the last century. While there is high inter-annual variability in the system, changes to the flooding regime over the last 20 years suggest that the wetland will become more persistent in response to increased frequency and intensity of extreme rainfall events for the region, which in turn will likely impact on the structure and functioning of this highly specialized ecosystem.

1 Introduction

Extreme climatic events such as tropical cyclones, heavy rainfall and severe drought are projected to become more intense and less frequent globally over the next hundred years in response to anthropogenic-driven climate change (Coumou and Rahmstorf, 2012). Tropical cyclones (TC) have been increasing in intensity in the semi-arid northwest of Australia since the 1970's, although trends in both their occurrence and the distribution of associated rainfall remain unclear (Hassim and Walsh, 2008; Goebbert and Leslie, 2010; Emanuel, 2013; Wang et al., 2013). Instrumental data and modelling suggest that the subtropical region has also experienced an increase in summertime rainfall since 1950 and overall wettening (Shi et al., 2008; Taschetto and England, 2009; Fierro and Leslie, 2013). Rainfall anomalies over the 1919–1999 period retrieved from tree ring records provide further evidence of a post-1955 wettening trend in northwest Australia (Cullen and Grierson, 2007). This wettening, since at least the 1980's, has been attributed to increased occurrence of monsoonal lows and TCs (Berry et al., 2011; Lavender and Abbs, 2013) and is also consistent with increases in extreme wet and hot conditions during the summer monsoon period in the Australian tropics over recent decades (Gallant and Karoly, 2010).

However, resultant impacts of shifts in hydroclimate on catchment hydrology are still poorly understood. Quantifying the "hydroclimatic expression" of regional events remains challenging for not only the Australian northwest but for arid environments more generally; these regions are often characterised by extreme hydroclimatic conditions, where rainfall is highly heterogeneous in its distribution and the majority of streams and rivers are ephemeral but highly responsive to intense rainfall events. For example, peak surface flow rates generated from ephemeral rivers and creeks in the Pilbara region of northwest Australia can reach thousands of cubic metres per second after such events (WA Department of Water, 2014). These factors contribute to high spatial and temporal heterogeneity of recharge-discharge mechanisms across any one catchment, which in turn presents considerable challenges for prediction of consequences of changes in

intensity and frequency of extremes. The consequences of intensification and shifts in frequency of the hydrological cycle as well as greater variability of precipitation patterns have already been documented in other parts of the world, including alterations in the seasonality and extent of floods or drought (Harms et al., 2010; Feng et al., 2013).

Ecological disturbances such as flood and drought cycles are usually described by their extent, spatial distribution, frequency (or return interval), predictability and magnitude (i.e., severity, intensity and duration) (White and Pickett, 1985). Determining how altered hydrologic regimes (floods and droughts) may in turn impact vulnerable ecosystems, including wetlands, requires detailed understanding of the links between the distribution of precipitation and flows across multiple spatial and temporal scales. The Pilbara region of northwest Australia, in common with other hot arid regions of the world including the Indian Thar, Namib-Kalahari and Somali deserts, is characterised by the most variable annual and inter-annual rainfall patterns on the planet (van Etten, 2009). In the case of the Pilbara, TCs and other low-pressure systems forming off the west Australian coast in the tropical Indian Ocean often result in extreme flooding events (WA Department of Water, 2014). These events punctuate years of prolonged drought, which together define the "boom-bust" nature of productivity in highly variable desert ecosystems (McGrath et al., 2012). Surface water availability or persistence of water features, physical disturbances and hydrological connectivity resulting from this highly dynamic regime play a central role in shaping aquatic and terrestrial ecosystem processes, species life history strategies and interactions and population dynamics (Box et al., 2008; Leigh et al., 2010; Pinder et al., 2010; Sponseller et al., 2013). Changes in hydroclimatic patterns and extremes that might alter the natural disturbance regime would thus have profound consequences for the structure and functioning of often highly specialised and adapted arid ecosystems (Newman, 2006; Leigh et al., 2010). However, while the ecological response to extreme flood or drought has been documented for several arid and semi-arid river basins, characterization of the disturbance regime has focussed primarily on the rivers only, and generally

been qualitative and coarsely resolved both temporally and spatially (Kennard et al., 2010; Mori, 2011; Stendera et al., 2012).

Remote sensing has proven to be the most suitable and often only tool for investigating spatial and temporal variability of arid zone remote wetlands (e.g., McCarthy et al., 2003; Bai et al., 2011; Thomas et al., 2011), as well as understanding ecohydrological processes (Gardelle et al., 2010; Haas et al., 2011; McGrath et al., 2012). As interannual variability of rainfall is high in arid regions, long temporal series are essential to capture the background variability of systems at appropriate temporal scales (Mori, 2011). High temporal resolution is also needed to accurately characterise the seasonal cycles and mechanisms generating the complex spatial and temporal patterning of floods at basin and regional scale and to effectively address the consequences of changes in disturbance regimes for different ecosystems. For example, satellite imagery has recently been successfully combined with hydrological modelling to extend wetland flood regime records from tropical Australia (e.g., Karim et al., 2012) and to investigate mechanisms such as connectivity among floodplains (e.g., Trigg et al., 2013). Similar approaches have also been used to understand the evolution of daily flood and dynamics of floodplain vegetation on the east coast of Australia (Powell et al., 2008). Remote sensing techniques have also been utilised to calibrate hydraulic models of dynamic flow processes during floods, albeit over relatively short time periods (e.g., Bates, 2012; Neal et al., 2012; Wen et al., 2013). However, flood regime analyses based solely on remotely-sensed data do not adequately capture the lengthy temporal scales of flood and drought cycles in many arid and semi-arid regions, which require calibration periods that encompass variability at interannual, decadal and multidecadal scales, especially to elucidate relationships with climatic drivers and geomorphological processes (Roshier et al., 2001; Viles and Goudie, 2003).

Here, we sought to identify the main hydroclimatic determinants of flooding regimes at the catchment scale and to establish the background of variability of surface water expression over the last century in the semi-arid northwest of Australia. First, we identified the main rainfall variables influencing surface water expression on the Fortescue

Marsh, the largest internally draining wetland in the Pilbara region (Fig. 1), by combining monthly remote sensing imagery from the Landsat archive to instrumental data from 1988–2012 via multivariate linear modelling. Second, we used the model to extend the flooding regime record of the Marsh to the 1912–2012 period based on instrumental records of rainfall. The development of this high-resolution temporal series allowed us to explore and better understand the factors governing surface water expression in a semi-arid landscape at multiple temporal scales, and particularly the significance of extreme events. These larger temporal windows are needed to better understand long-term functioning of arid zone wetlands such as the Marsh but more broadly to establish improved context for more informed water management strategies in these sensitive regions.

2 Methods

2.1 Study site – the Fortescue Marsh

The Fortescue Marsh (hereon referred to as the Marsh; Fig. 1) is an ephemeral wetland of some 1300 km^2, which is comprised of a complex network of riverine floodplains and freshwater and floodplain lakes. The Marsh is the largest wetland of inland northwest Australia and formally recognised as nationally significant for its ecological and hydrologic values (Environment Australia, 2001; McKenzie et al., 2009; Pinder et al., 2010). Vegetation across the Marsh is dominated by salt-tolerant chenopod (*Tecticornia*) shrublands, with eucalypt and Acacia woodlands growing adjacent to the most permanent water features (Beard, 1975). As the largest freshwater feature for hundreds of kilometres, the Marsh is also of considerable heritage significance including as a key focus for aboriginal communities for more than 40 000 years and since the late 1800's for early European pastoralists (Slack et al., 2009; Law et al., 2010; Barber and Jackson, 2011).

The Marsh acts as an internally draining basin for the 31 000 km^2 upper Fortescue River catchment (21–23° S; 119–121° E; Fig. 1). The flood level required for the Marsh to overflow to the Lower Fortescue catchment is not formerly established but digital elevation models (Geosciences Australia, 2011) suggest water could flow if inundations reached > 410 m a.s.l. The upper Fortescue River is the main drainage of the catchment, flowing north to northwest into the wetland system. Flow in the Fortescue River is characterized as "variable, summer-dominated and extremely intermittent" (Kennard et al., 2010), where very large volumes of runoff are generated following heavy rainfall, which is in contrast with the empty beds of the dry season (WA Department of Water, 2014). The Ophthalmia Dam, constructed on the Fortescue River at Newman in 1981 to provide the town with drinking water, has a 32 GL capacity and receives from a relatively small and low lying fraction of the catchment (14.5 %) with minimal observed impact on the riverine ecosystem at the mouth of the Marsh (Fig. 1; Payne and Mitchell, 1999).

The Fortescue River Valley paleodrainage, eroded from the Hamersley Basin sedimentary rocks, lies between the Hamersley Range in the south and the Chichester Range in the north, constituting the main topographical features of the Eastern Pilbara (Dogramaci et al., 2012). The Fortescue Marsh consists of colluvial and alluvial sedimentary deposits up to ∼ 50 m developed on the top of the Oakover Formation, a sequence of younger Tertiary lacustrine carbonate, silcrete and mudstone rocks deposited in the Fortescue River Valley (Clout, 2011). The Oakover Formation is underlain by fractured dolomite and shale of the Wittenoom Formation (Clout, 2011). The recent sediments consist mainly of detrital clays, iron oxides and gypsum. The alluvial and colluvial aquifers of the Fortescue Marsh are frequently confined by impermeable consolidated massive clays and calcrete and silcrete layers. The residence time of water in the upper sections of the catchment is short: surface runoff is high via the steep gradients of creeks and gorges. The groundwater under the Marsh is highly saline and likely developed by evaporation of floodwater and consequent recharge to underlying aquifers (Skrzypek et al., 2013). The most reported permanent water feature on the

Marsh is 14 Mile Pool, located at the mouth of the upper Fortescue River; this pool does not retain water significantly diluted nor flushed by groundwater, which contrasts to other small through-flow pools in upper parts of the secondary tributaries of the catchment (Fellman et al., 2011; Skrzypek et al., 2013).

2.2 Climate and rainfall patterns

Over the 1912–2012 historical period, the upper Fortescue River catchment received on average 290 mm yr^{-1}, of which 75 % fell during the monsoonal summer (November–April) (Fig. 2a; Australian Bureau of Meteorology, www.bom.gov.au/cgi-bin/silo/cli_var/area_timeseries.pl). "Meteorologically dry" years received less than 200 mm rainfall, while "wet" years received over 300 mm (Fig. 2a), as defined by the left-skewed mode of the yearly rainfall frequency distribution (35 % of all years). Scattered, small-scale storms cause daily rainfall to be highly variable among the 17 weather stations (Fig. 1a, Appendix A, Table 1) of the upper Fortescue River catchment (www.bom.gov.au/climate/data/). Evaporation is highest during the summer and generally exceeds rainfall (Skrzypek et al., 2013); average temperatures in summer range between 30–40 °C, and in winter months between 24–35 °C (www.bom.gov.au/climate/data/).

Heavy summer storms and tropical cyclones often generate large floods in the major river systems of the Pilbara, particularly on the coast, while winter rainfall is typically not sufficient to generate surface flows (Fig. 2; WA Department of Water, 2014). Numerous historical tracks of cyclones have been recorded in the upper Fortescue River catchment during the last century (www.bom.gov.au/cyclone/history/). When TC tracks were recorded within a 500 km radius of the Marsh, total monthly rainfall in the catchment was significantly greater (p value < 0.01) than the 1912–2012 monthly averages for no-TC months (Fig. 2b). Rain intensity during TC months was also higher (17–22 mm monthly rain rain d^{-1}) than in no-TC months (8–10 mm monthly rain rain d^{-1}). Not surprisingly, extremes in the rainfall record (defined here as exceeding the 95th and 99th percentile of all monthly total rainfall occurrences, or Ex_{95} and Ex_{99}, respectively) are linked to the occurrence of tropical cyclones. In fact, half of the months falling in the

Ex_{95} (i.e., > 104 mm rainfall/month) recorded at least one TC (30 out of 60 months). Further, at least one TC occurrence was recorded for nine out of 12 months falling in the Ex_{99}, i.e., months recording 190–258 mm of rainfall.

2.3 Mapping flood history based on the Landsat archive (1988–2012)

We mapped the flood history (i.e., surface water expression) of the Marsh floodplain area (~ 1300 km^2; Fig. 1) between 1988 and 2012 from high-resolution (i.e., ca. two-week intervals) Landsat images that captured patterns of surface water expression (see Appendix A, Sect. A1 for details). The Marsh floodplain area is defined here as elevations below 410 m a.s.l. and within the upper Fortescue River catchment (Fig. 1). Surface water features were extracted from Landsat images using an automated thresholding method in *ArcGIS* v. 9.2 and flood areas (F_A) were calculated using *Fragstats* v. 4.1 (see Appendix A, Sect. A2 for details). We calculated potential errors associated with using the pixel resolution (30 m) of Landsat images and the thresholding approach to classify surface water features (see Appendix A, Sect. A2 for details). Based on these potential errors, estimated monthly change in flood area (ΔF_A) of less than 6 km^2 should be considered with caution. However, given the scale of variation in F_A on the Marsh (ca. 0–1100 km^2, Fig. 3) this error is relatively small. To provide further confidence in our dataset within the estimated errors we used two 40 cm digital ortho-images produced from aerial photographs taken in July 2010, April 2012 (Fortescue Metals Group Limited, Perth, Australia) and one 5 m resolution image taken in August 2004 (Landgate, Government of Western Australia), to confirm that our flood areas mapped from Landsat images taken on similar dates (i.e., within one week of the ortho-image dates) were within 1 pixel (30 m) of the flood area visible in the ortho-images. A groundtruthing expedition from the dry season (November 2012) and a helicopter delineation of the inundation plume in the wet season (February 2012) were also conducted.

2.4 Modelling floodplain wetting and drying events

2.4.1 Model development and selection

Of the 493 Landsat images processed, only 208 images (TM & ETM) were used to build a calibration dataset for hydrological modelling between the 1988–2012 period (Fig. 3). Following selection of the latest observation for each month (or of the first observation of the next month if within the first week; n = 265), only ΔF_A between two consecutive months (n = 232) that were above the estimated errors were included. As a result, 160 ΔF_A values were used in the final calibration dataset. Most (70 %) ΔF_A values were calculated over a ca. month-long interval (i.e., 30 ± 7 d), but this interval ranged from 16 to 48 days for the full calibration dataset.

We used a multiple linear regression (in *R* v. 2.11.1) to identify the main climatic drivers of ΔF_A on the Marsh and generate a predictive model to reconstruct monthly F_A for the last century (1912–2012). Climatic variables tested as predictors in the model included: monthly total rainfall, number of rain days, mean temperature and potential evapotranspiration calculated from weather station records and monthly gridded datasets (see Appendix B, Table A2 for details). To account for the potential effect of system memory, we included F_A in the previous 1 to 12 months as predictors in the model. Variables that were significant in explaining the variation in F_A, provided the best fit as per the adjusted coefficient of variation (R^2_{adj}) for the number of variables and the smallest root mean square error E_{RMS} were used in the final model.

2.4.2 Validation of model and 1912–2012 reconstruction

The model's predictive accuracy was tested by both cross-validation and calculation of the E_{RMS} of prediction (E_{RMSP}). A random ten-fold cross-validation (CV) was computed using the CVlm function of the DAAG R package v. 1.16 (Maindonald and Braun, 2013). The E_{RMSP}, which indicates how well the model fits an independent subset of

the data, was obtained by removing block subsets representing a third of the calibration occurrences (i.e., 1988–1997; 1998–2004; 2005–2012).

We used the modelled ΔF_A to reconstruct the total area flooded (F_A) from the earliest available instrumental data in the region, i.e., from March 1910 to December 2012. However, the value of F_A in March 1910 being unknown, the observed F_A minimum, average and maximum of the calibration period (1988–2012) were used as starting points and long-term statistics for the hydrological regime were calculated from the meeting point of the three time series, i.e., January 1912. Yearly statistics were calculated for the rain year, i.e., November–October. We used comparisons with an aerial photographic survey from 1957 (Edward de Courcy Clarke Earth Science Museum, UWA), early MSS Landsat imagery (1972–1988) and droughts/flood events reported by early surveyors and pastoralists to local newspapers (www.trove.nla.gov.au) to provide historical anchors to our 1912–2012 time series (see references in-text).

3 Results and discussion

3.1 Hydroclimatic determinants of floods and droughts

Total rainfall in the upper Fortescue River catchment (R), number of rain days (R_d) and carried-over inundated area (F_{At-1}) were the strongest hydroclimatic determinants of the monthly flooding and drying (ΔF_A) regime at the Fortescue Marsh (p value < 0.001; Table 1). The high R^2_{adj} (0.79, p value < 0.001) indicates that the final model included the most important contributors to ΔF_A variation. The model's predictive accuracy was similar for both tests performed, i.e., the E_{RMSCV} and the best E_{RMSP} = 56 km^2. However, the subset model used to calculate E_{RMSP}, which excluded the particularly wet and variable 1998–2004 period from the calibration period, performed the worst at reconstructing ΔF_A for the 1998–2004 verification period (R^2_{adj} = 0.64; E_{RMSP} = 86 km^2), indicating this period constituted an important range for the calibration of the model. Both other calibration models (excluding the 1988–1997 or the 2005–2012 periods)

were more accurate (E_{RMSP} = 58 and 56 km^2, respectively), and the overall variance explained improved to 81 and 82 % when either of these dry, less variable periods was removed from the model.

The enhanced performance of the subset models built without as many "dry" periods highlights an important limitation of the observation dataset. Because it was not possible to calculate ΔF_A from the calibration set when the surface water at the Marsh was dry, water loss, i.e., soil water storage depletion, was therefore underestimated during these periods. Concurrently, however, the reconstruction of monthly F_A values below 0 km^2 reflects the ability of our model to provide quantitative information on soil water storage, or the unsaturated zone of the Marsh where rapid infiltration of rainwater was observed following heavy rainfall at the Marsh (Skrzypek et al., 2013). This zone between water table and ground surface likely acts as a buffer to net surface water gain or loss. For further details on the modelling statistics, refer to the Pearson correlation matrix for the modelled variables (Appendix A, Table A3) and the distribution of observed against reconstructed ΔF_A values (Appendix A, Fig. A1).

The goodness-of-fit and relatively small errors of the model provide confidence in the reconstruction starting in the early 1900's. In particular, the inclusion of R_d in addition to R makes the model and reconstruction robust against the recorded changing rainfall intensity over the century (Shi et al., 2008; Taschetto and England, 2009; Gallant and Karoly, 2010; Fierro and Leslie, 2013). However, the model tended to underestimate ΔF_A following very intense rainfall events (large rainfall over 1–3 days), which might be partly attributed to the monthly resolution (Appendix A, Fig. A1). Reconstructed values of ΔF_A for any given month are calculated for the last day of the month and as such do not account for the timing of intense events during that month. A large rainfall event occurring early in the month would thus result in smaller ΔF_A. The underestimation of ΔF_A values during intense events might also be due to the high spatial heterogeneity of rainfall in the catchment, which was readily apparent when events were much larger closer to the Marsh (e.g., Marillana Station, Fig. 1b; www.bom.gov.au/climate/data/). Consequently, our time series mostly reflects regional-scale events rather than more

localised events. The use of weighted contributions of the different meteorological stations or sub-catchments within the upper Fortescue River catchment might improve the downscaling of this model. However, the instrumental records in this region are both temporally and spatially patchy, and using higher resolution gridded data would not necessarily truly improve the resolution of the data evenly for the last century (Fig. 1; www.bom.gov.au/climate/data/).

Severe and intense rainfall events (i.e., high R and low R_d) clearly drive the hydrologic regime of this system over the last century. Total rainfall contributed most ($R_\beta = 145\,km^2$; p value < 0.001) to monthly flooding of the Marsh (ΔF_A). More than 75 mm rain/month in the catchment systematically caused a net wettening (increase in F_A) of the Marsh's floodplains while < 30 mm rain month^{-1} was generally insufficient to impact on F_A (Fig. 4). However, more intense rainfall events resulted in much larger flooding episodes. Conversely, for the same total rainfall, more rain days in the month strongly dampened the extent of floods ($R_{d\beta} = -63\,km^2$; p value < 0.001). These "flash floods" drive the current hydrological regime of the Marsh but are also consistent with the hydrochemical evolution and modern recharge of shallow groundwater under the Marsh (Skrzypek et al., 2013). By washing down of surface salts deposited on the Marsh during previous evaporation episodes, large floods not only recharge the system, but also deliver freshwater that becomes available at surface for extended periods of time. This heavy rainfall (as opposed to groundwater) driven system is rather unusual in the arid zone, where many wetlands are groundwater-dominated, playa-like ecosystems (Bourne and Twidale, 2010; Tweed et al., 2011). In arid zone playas, the hypersaline groundwaters from the deep aquifer are connected to surface processes and result in saline waters being exposed (Bourne and Twidale, 2010; Cendon et al., 2010). In contrast, our results support that the Fortescue Marsh is rather a paleosaline lake where vegetation can grow and surface water is largely fresh, but then eventually becomes brackish due to the concentration of solutes with time owing to evaporative losses.

The sequence of events, or the "system memory", was also an important determinant of surface water availability on the Marsh. When still inundated from the previous month ($F_{At-1} > 0\,km^2$), decrease of the total area flooded was significantly larger ($F_{At-1\beta} = 29\,km^2$; p value < 0.001). For example, although the largest inundated area was recorded in 2000, the 1942 net ΔF_A was larger but resulted in slightly less inundated area at the Marsh owing to the drier conditions than in 1999 in the previous month. Intervals (Int) between observations (number of days over which the change was observed) did not significantly improve the fit of the model ($Int_\beta = -8\,km^2$; p value = 0.07). This variable (Int) thus rather acted as a constant that contributed to the decrease of surface water every month. Unsurprisingly, cumulative severe floods resulted in the longest inundation periods recorded on the Marsh, and often contributed to the following year's hydrological status. Over the 1912–2012, 32 % of years had up to 400 km^2 (40 % fullness) surface water expression carried over to the next year (i.e., winter to summer). In contrast, 68 % of years ended with no surface water and depleted aquifers in October (Fig. 5b).

Our findings indicate that the reconstructed total area flooded at the Marsh represents an integrated ecohydrological catchment response to rainfall, which is expected from such terminal basins (Haas et al., 2011). We observed that the impact of rainfall on floods and droughts is at least in part modulated by the high local evaporation rate (five to ten-fold greater than rainfall), which acts as a constant drying force on the surface water even though temperature or potential evapotranspiration (PET) did not significantly improve the fit of the model. In addition, vegetation in drylands typically shows a rapid increase in productivity in the few months following a large rainfall event (e.g., Veenendaal et al., 1996; McGrath et al., 2012); thus, runoff from subsequent events might be dampened through enhanced physiological (plant water) use, which is in turn consistent with the negative effect of F_{At-1} on flood area change (Table 1). We suggest that expected seasonal and interannual variation in temperature and/or PET were thus largely accounted for through the use of F_{At-1} and the constant *Interval* variables.

3.2 Spatial and temporal patterns of inundations

Our monthly reconstruction reveals that the floodplains of the Fortescue Marsh have had extremely variable interannual severity of total flooded area (F_{Amax}) that in turn determined the duration of inundations for the last century (Fig. 3). Of the last 100 years (1912–2012), almost 25 % were large flood years, i.e., years for which the maximum flood area (F_{Amax}) was over 300 km^2 (Fig. 3b). Large inundations typically occurred as a result of one to three month long flood pulses in the austral summer (February–April). As described earlier, these flood pulses were mainly associated with regional hydroclimatic events such as TC occurring in the austral summer (January–March), and are major drivers of surface water expression at the Marsh for the last century. Following large floods, some level of inundation could be maintained for over 12 months in 7 % of years (Figs. 6 and 7). Further, only large flood years generated substantial > 0.5 m depth of surface water (Fig. 8a), which would also have the potential to completely submerge the vast chenopod community on the Marsh (Beard, 1975). These large flood years, their consequent supra-seasonal sustained inundations and their connectivity to the western sections (downstream) have been relatively frequent over the last century and reflect the natural variability in the hydroclimatic regime. On the other hand, > 800 km^2 flood years (only two in the past 100 yr, 1942 and 2000) are considered extreme, infrequent disturbances bringing exceptional volumes of freshwater to the system (Fig. 8b). The most striking effect of the interannual system memory was observed between 1999 and 2006, the period during which inundations extent and duration on the Marsh were above average and unprecedented for the last century. The longest period in the last 100 years that surface water was consistently present on the Marsh (i.e., $F_A > 0$ km^2) was from 1998 to 2002, including the largest yearly inundation for the entire century in March 2000 of $\sim$ 1000 km^2 (Fig. 3c).

In addition to the large flooding events described above, the majority of years (70–79 %) experienced at least one month of inundation resulting from smaller floods (F_{Amax} < 40–48 km^2) (Figs. 6 and 7) that in turn also influenced the distribution and

connectivity of surface water within the different sections of the Marsh (Fig. 6). During large or severe inundation years, the entire floodplain became initially one (Fig. 6). Following such an event in 1934, pastoralists experienced the "Marsh becoming a [400 km^2] large lake" (Fig. 6; Aitchison, 2006). Going into the winter months, evaporation and the lack of significant input from rainfall events typically resulted in drying and progressive formation of disconnected pools mainly along the northern shore and eastern end of the Marsh (Fig. 6). Based on our 25 yr calibration period, similarly severe years resulted in spatially consistent patterns of interannual inundation during both wetting and drying phases (Fig. 6). While quite frequent, large flood years do not occur at regular intervals, conferring a poor predictability to surface water in the system. The lowest recurrence was prior to 1960, with up to 14 years between two events; post 1960, large events have occurred at intervals of seven years or less, which in turn has resulted in more severe and prolonged inundations e.g., between 1999 and 2006.

The increased flood severity and duration over recent decades relative to the previous 80 or so years observed in our flooding record is consistent with the increasing trend in heavier summer rainfall events recorded in the region for the same period (Shi et al., 2008; Taschetto and England, 2009; Gallant and Karoly, 2010; Fierro and Leslie, 2013). A simple linear regression between time and yearly duration of floods ($F_A > 0$ km^2) further demonstrates slightly increased inundation length since the beginning of the century (p value = 0.046). However, the significance of this finding should be treated with some caution given the non-independence of the F_{Amax} (especially between two consecutive years) and the limited number of observations included (n = 25 flooding events). The appraisal of multi-decadal trends in the hydrological regime could be improved by exploring the impact of cyclicity of known larger scale climatic drivers of (summer) rainfall in the northwest of Australia such as the El Niño–Southern Oscillation (ENSO), the Indian Ocean Dipole (IOD) and the Madden–Julian oscillation (MJO) – phasing of these different modes (Risbey et al., 2009). The development and application of high-resolutions proxy indicators of past hydroclimatic changes for the arid

zone could also provide more robust insights on multi-decadal trends and ecosystem vulnerability to these changes (e.g., Cullen and Grierson, 2007).

3.3 Significance of predictability and persistence of drought

Our reconstruction shows that the Fortescue Marsh floodplains have more often been dry than wet over the last century (Fig. 3c). Droughts of at least one year were frequent (21 %) between 1912–2012 (Figs. 3c d, and 7). The most recent drought that persisted for more than 2 years occurred between 1990 and 1993 (3.2 years). In contrast, particularly extended drought periods (where no surface water is evident on the Marsh) were more frequent between the late 1930's and early 1960's, with the longest supraseasonal drought on record lasting 4.3 years (between 1961 and 1965). In such water-restricted and remote environments, early pastoralists would have been the first to notice changes in the distribution and availability of freshwater. Reports of "bad drought" on Roy Hill Station in early 1939 and winter of 1940, where "no feed" for cattle was available (Aitchison, 2006) corroborate our reconstruction. Dramatic vegetation changes were also documented on the Marsh's floodplain during this dry period (1938–1940), which coincided shortly after with Marillana Station shifting from cattle to sheep farming (Aitchison, 2006). In our time series, this documented drought corresponded to largely dry conditions ($F_{Amax} < 150\,km^2$) at the Marsh due to the occurrence of only minor flood events over these years (Fig. 3c). A 20 month period between 1918 and 1919 where F_A at the Marsh was reconstructed as less than $0\,km^2$ in our analysis also corresponds to a report by the Roy Hill Pastoral Company, one of the main pastoralist in the upper Fortescue River catchment, as a "severe drought" causing the installation of "10 new wells" in 1919 (Dept Land and Survey, 1919) (Fig. 3c).

Overall, the eastern section of the Marsh experienced the least interannual variability by holding the most reliably inundated freshwater areas (Fig. 6), consistent with the presence of long-lived trees at 14 Mile Pool and Moorimoordinia Native Well (Beard, 1975). The September 1957 aerial photograph also shows these pools partially filled even though there was little summer rain that year, also corroborating our

reconstruction of a dry period at that time. These more permanent, shallow water features were restricted to the floodplains at the mouth of the upper Fortescue River and other smaller tributaries draining the steeper slopes of the Chichester Range to the north (Fig. 6). These sections have thus been under a more localised and "high" inundation frequency regime from smaller events (Thomas et al., 2011; Fig. 6). These sequential, smaller events potentially maintain refugia for aquatic populations, which may facilitate recolonisation of other parts of the Marsh following the larger, less frequent flood disturbances that in turn effectively "reset" arid zone ecosystems (Leigh et al., 2010; Stendera et al., 2012). With such spatial variation in floods frequency, we can also expect vegetation communities on the Marsh to form mosaics tightly linked to their different water requirements and tolerances, as has been seen on other floodplains such as those of the Macquarie Marshes in central-eastern Australia (Thomas et al., 2011).

4 Conclusions

We developed a robust model to predict and characterize the surface water response of a major regional wetland to hydroclimatic variability over the last century. Our approach is readily applicable to extend the temporal record to other ephemeral water bodies. Through greater understanding of system responsiveness to regional rainfall patterns, we also now have improved capacity to assess the long-term ecohydrological functioning of arid floodplains. For example, if current rainfall trends are sustained, increased flooding of the Fortescue Marsh will prolong the inundation period in the year, the connectivity between the different parts of the Marsh and the river network and increase the carry-over for the following year. The resulting enhanced persistence may in turn affect long-term hydrochemical and ecological processes of the system, e.g., by an increase in surface water salinity.

Appendix A: Mapping the flood history

A1 Landsat archive/image selection

The flood history of the Fortescue Marsh was reconstructed using standard terrain corrected scenes for systematic radiometric and geometric accuracy (Level 1T) from the USGS EarthExplorer Landsat archive (http://earthexplorer.usgs.gov/). The Landsat archive has seasonal to monthly coverage of the Fortescue Marsh from 1972–1988 and fortnightly coverage from 1988–2012. We quantified water coverage, or total flooded area (F_A) from a subset of 493 satellite images with the analysis of wavelengths sensitive to water reflectance (Xu, 2006), specifically the short wave (SWIR) or mid infrared (MIR) radiation bands 5 (TM, ETM) and 3 (MSS). All image processing was conducted using ArcGIS v.9.2 and ERDAS Imagine 2011. Pixel resolution was 30 m × 30 m (900 m^2) for the observation period (1988–2012).

A2 Flood area delineation and error

Water features were relatively straightforward to extract using a simple automated thresholding method (Xu, 2006), owing to their very high contrast to the surrounding arid landscape. F_A could not be estimated using our automated method when partial cloud cover was present in the satellite imagery, or for the ETM-SLC off series of Landsat 7 (169 images from a total of 493). Therefore, F_A was estimated in these years by calculating the midpoint between the most recent "before and after" F_A estimates. This approach also allowed us to capture the largest F_A estimates as they were often partly obstructed by clouds.

To account for registration error across the temporal and satellite series, the F_A estimate and its associated error (*estimation errors*) were obtained from three water features extracted for every image using a lower, mid and upper threshold of reflectance values. The three consecutive threshold values (either 10, 20, 30, 40, 50, or 60 value of reflectance) were selected to include the highest frequency distribution of water pixels

while providing the smallest F_A estimate error. We also calculated *resolution errors* in extracting F_A to account for the use of 30 m × 30 m pixels values. Here, we applied a 15 m buffer inside and outside the water-only polygon for all thresholds. Thus, *estimation* and *resolution errors* were largest when F_A was small owing to an increase in the "edge length" to size ratio, and differences in F_A less than 6 km^2 should be considered with caution. A simple linear regression obtained between the automated F_A and its buffer was used to calculate the resolution error for these shapes. The *resolution error* for shape-estimated F_A was calculated using linear regression formulas obtained between F_A and inside buffer (R^2 = 0.99, p value < 0.001) and outside buffer (R^2 = 0.99, p value < 0.001). Strong congruency between elevation contours and the shape of flooded area estimates on the Fortescue Marsh indicate that our thresholding methodology accurately detected standing water. Neither *estimation* nor *resolution errors* were found to follow a seasonal or overall temporal trend. However, we cannot discount that areas of waterlogged ground also contributed to the estimates of flooded area (Castaneda et al., 2005).

Appendix B: Climate variables

While 17 meteorological stations have been intermittently recording daily rainfall data in the upper Fortescue River catchment, only six are currently still in operation, forming a too sparse and temporally inconsistent network for direct use in this study (Fig. 1; Table A1). Explanatory hydroclimatic variables were thus generated using monthly gridded datasets resolved at either 0.5 or 1° cell size weighted for their relative contribution to the upper Fortescue River catchment (Table A2). Total rainfall and mean temperature were obtained from the Australian Bureau of Meteorology (www.bom.gov.au/cgi-bin/silo/cli_var/area_timeseries.pl), the Climatic Research Unit (CRU) and the Global Precipitation Climatology Centre (GPCC) via the Koninklijk Nederlands Meteorologisch Instituut (KNMI) Climate Explorer (climexp.knmi.nl). Potential evapotranspiration (PET), calculated using Penman–Monteith parameterization and

based on the actual vegetation cover, was from van der Schrier et al. (2013). The mean number of rain days/month (R_d) was calculated from daily rainfall records obtained from the four meteorological stations still in operation, located within or closest the upper Fortescue River catchment, relatively well spread in the vast geographic area and with the longest records (i.e., Noreena Downs, Bulloo Downs, Marillana and Mulga Downs) (Fig. 1; Table A1).

Author contributions. A. Rouillard wrote the paper with input from P. F. Grierson, G. Skrzypek, C. Turney and S. Dogramaci. A. Rouillard collected and processed the satellite imagery and conducted the statistical analyses. A. Rouillard and G. Skrzypek developed the modelling approach after discussion with co-authors. The study was conceived by P. F. Grierson, A. Rouillard, G. Skrzypek, S. Dogramaci and C. Turney.

Acknowledgements. This research was supported by the Australian Research Council (ARC) in partnership with Rio Tinto (LP120 100 310). A. Rouillard was supported by the Australian Government and UWA via an International Postgraduate Research Scholarships (IPRS) and an Australian Postgraduate Awards (APA), as well as by the Canadian and Québec governments via a Natural Sciences and Engineering Research Council (NSERC) and a Fonds québécois de la recherche sur la nature et les technologies (FQRNT) via graduate scholarships. G. Skrzypek participation is supported by an ARC Future Fellowship (FT110 100 352). We thank the Fortescue Metals Group Ltd for access to ortho-images and Digital Elevation Model of the Fortescue Marsh. The authors thank Jeremy Wallace (CSIRO) and Victoria Marchesini (UWA) for advice on image processing, Gerard van der Schrier (KNMI) for sharing the PET dataset, Gavan McGrath (UWA) for council on tropical cyclones, Caroline Bird (Archae-Aus) for help with archival research and the following researchers for their assistance with the modelling: Yun Li (CSIRO), Jérôme Chopard (UWA), Michael Renton (UWA), Edward Cook (UColumbia), Jonathan Palmer (UTAS) and Jason Smerdon (UColumbia). We also acknowledge the kind support of Lee and Sue Bickell (Marillana Station), Barry and Bella Gratte (Ethel Creek Station), Victor and Larissa Gleeson (Mulga Downs Station), and Murray and Ray Kennedy (Roy Hill Station). We are also grateful to Alison O'Donnell and Gerald Page for providing useful comments on the early version of the manuscript.

References

Aitchison, G. P.: "I've Had a Good Life" Phil's Story: The Autobiography of a Pilbara Pioneer, Western Australia, Hesperian Press, Carlisle, 48 pp., 2006.

Bai, J., Chen, X., Li, J., Yang, L., and Fang, H.: Changes in the area of inland lakes in arid regions of central Asia during the past 30 years, Environ. Monit. Assess., 178, 247–256, 2011.

Barber, M. and Jackson, S.: Water and Indigenous People in the Pilbara, Western Australia: a Preliminary Study, CSIRO: Water for a Healthy Country Flagship Report, Darwin, 104 pp., 2011.

Bates, P. D.: Integrating remote sensing data with flood inundation models: how far have we got?, Hydrol. Process., 26, 2515–2521, 2012.

Beard, J. S.: The Vegetation of the Pilbara Area, Vegetation Survey of Western Australia, 1 : 1 000 000 Vegetation Series, Map and Explanatory Notes, The University of Western Australia Press, Nedlands, 1975.

Berry, G., Reeder, M. J., and Jakob, C.: Physical mechanisms regulating summertime rainfall over northwestern Australia, J. Climate, 24, 3705–3717, 2011.

Bourne, J. A. and Twidale, C. R.: Playas of inland Australia, Cad. Lab. Xeol. Laxe, 35, 71–97, 2010.

Box, J. B., Duguid, A., Read, R. E., Kimber, R. G., Knapton, A., Davis, J., and Bowland, A. E.: Central Australian waterbodies: the importance of permanence in a desert landscape, J. Arid Environ., 72, 1395–1413, 2008.

Castaneda, C., Herrero, J., and Auxiliadora, C., M.: Landsat monitoring of playa-lakes in the Spanish Monegros desert, J. Arid Environ., 63, 497–516, 2005.

Cendon, D. I., Larsen, J. R., Jones, B. G., Nanson, G. C., Rickleman, D., Hankin, S. I., Pueyo, J. J., and Maroulis, J.: Freshwater recharge into a shallow saline groundwater system, Cooper Creek floodplain, Queensland, Australia, J. Hydrol., 392, 150–163, 2010.

Clout, J. M. F.: The Roy Hill Project, AisIMM, 3, 52–65, 2011.

Coumou, D. and Rahmstorf, S.: A decade of weather extremes, Nat. Clim. Change, 2, 491–496, 2012.

Cullen, L. E. and Grierson, P. F.: A stable oxygen, but not carbon, isotope chronology of Callitris columellaris reflects recent climate change in north-western Australia, Clim. Change, 85, 213–229, 2007.

Department of Land and Survey: “Surveys by Roy Hill Pastoral Co in Victoria district of Roy Hill Station”, ACC541, file 5125, Archive Collection of the State Records Office of Western Australia, 1919.
Dogramaci, S., Skrzypek, G., Dodson, W., and Grierson, P. F.: Stable isotope and hydrochemical evolution of groundwater in the semi-arid Hamersley Basin of subtropical northwest Australia, J. Hydrol., 475, 281–293, 2012.
Emanuel, K. A.: Downscaling CMIP5 climate models shows increased tropical cyclone activity over the 21st century, P. Natl. Acad. Sci. USA, 110, 12219–12224, 2013.
Environment Australia: A Directory of Important Wetlands in Australia, 3rd Edn., Environment Australia, Canberra, Australia, 157 pp., 2001.
Fellman, J. B., Dogramaci, S., Skrzypek, G., Dodson, W., and Grierson, P. F.: Hydrologic control of dissolved organic matter biogeochemistry in pools of a subtropical dryland river, Water Resour. Res., 47, 1–13, 2011.
Feng, X., Porporato, A., and Rodriguez-Iturbe, I.: Changes in rainfall seasonality in the tropics, Nat. Clim. Change, 3, 811–815, 2013.
Gallant, A. J. E. and Karoly, D. J.: A combined climate extremes index for the Australian region, B. Am. Meteorol. Soc., 23, 6153–6165, 2010.
Gardelle, J., Hiernaux, P., Kergoat, L., and Grippa, M.: Less rain, more water in ponds: a remote sensing study of the dynamics of surface waters from 1950 to present in pastoral Sahel (Gourma region, Mali), Hydrol. Earth Syst. Sci., 14, 309–324, doi:10.5194/hess-14-309-2010, 2010.
Geoscience Australia (GA): 1 Second SRTM Derived Hydrological Digital Elevation Model (DEM-H) Version 1.0, Commonwealth of Australia, 2011.
Goebbert, K. H. and Leslie, L. M.: Interannual variability of Northwest Australian tropical cyclones, J. Climate, 23, 4538–4555, 2010.
Haas, E. M., Bartholomé, E., Lambin, E. F., and Vanacker, V.: Remotely sensed surface water extent as an indicator of short-term changes in ecohydrological processes in sub-Saharan Western Africa, Remote Sens. Environ., 115, 3436–3445, 2011.
Harms, T. K. and Grimm, N. B.: Influence of the hydrologic regime on resource availability in a semi-arid stream-riparian corridor, Ecohydrology, 3, 349–359, 2010.
Hassim, M. E. E. and Walsh, K. J. E.: Tropical cyclone trends in the Australian region, Geochem. Geophy. Geosy., 9, 1–17, 2008.

Karim, F., Kinsey-Henderson, A., Wallace, J., Arthington, A. H., and Pearson, R. G.: Modelling wetland connectivity during overbank flooding in a tropical floodplain in north Queensland, Australia, Hydrol. Process., 26, 2710–2723, 2012.
Kennard, M. J., Pusey, B. J., Olden, J. D., Mackay, S. J., Stein, J. L., and Marsh, N.: Classification of natural flow regimes in Australia to support environmental flow management, Freshwater Biol., 55, 171–193, 2010.
Lavender, S. L. and Abbs, D. J.: Trends in Australian rainfall: contribution of tropical cyclones and closed lows, Clim. Dynam., 40, 317–326, 2013.
Law, W. B., Cropper, D. N., and Petchey, F.: Djadjiling rockshelter: 35,000 14C years of Aboriginal occupation in the Pilbara, western Australia, Aust. Archaeol., 70, 68–71, 2010.
Leigh, C., Sheldon, F., Kingsford, R. T., Arthington, A. H.: Sequential floods drive “booms” and wetland persistence in dryland rivers: a synthesis, Mar. Freshwater Res., 61, 896–908, 2010.
Maindonald, J. and Braun, W. J.: DAAG: Data Analysis And Graphics data and functions, available at: www.stats.uwo.ca/DAAG/, 2013.
McCarthy, J. M., Gumbricht, T., McCarthy, T., Frost, P., Wessels, K., and Seidel, F.: Flooding patterns of the Okavango wetland in Botswana between 1972 and 2000, Ambio, 32, 453–457, 2003.
McGrath, G. S., Sadler, R., Fleming, K., Tregoning, P., Hinz, C., and Veneklaas, E. J.: Tropical cyclones and the ecohydrology of Australia’s recent continental-scale drought, Geophys. Res. Lett., 39, 1–6, 2012.
McKenzie, N. L., van Leeuwen, S., and Pinder, A. M.: Introduction to the Pilbara biodiversity survey, 2002–2007, Records of the Western Australian Museum, Supplement, 78, 3–89, 2009.
Mori, A. S.: Ecosystem management based on natural disturbances: hierarchical context and non-equilibrium paradigm, J. Appl. Ecol., 48, 280–292, 2011.
Neal, J., Schumann, G., and Bates, P.: A subgrid channel model for simulating river hydraulics and floodplain inundation over large and data sparse areas, Water Resour. Res., 48, 1–16, 2012.
Newman, B. D., Wilcox, B. P., Archer, S. R., Breshears, D. D., Dahm, C. N., Duffy, C. J., McDowell, N. G., Phillips, F. M., Scanlon, B. R., and Vivoni, E. R.: Ecohydrology of water-limited environments: a scientific vision, Water Resour. Res., 42, 1–15, 2006.
Payne, A. L. and Mitchell, A. A.: An Assessment of the Impact of Ophthalmia Dam on the Floodplains of the Fortescue River on Ethel Creek and Roy Hill Stations, Resource Management

Technical Report No. 124, Western Australian Department of Agriculture, Perth, Western Australia, 60 pp., 1999.
Pinder, A. M., Halse, S. A., Shiel, R. J., and McRae, J. M.: An arid zone awash with diversity: patterns in the distribution of aquatic invertebrates in the Pilbara region of Western Australia, Records of the Western Australian Museum, 78, 205–246, 2010.
Powell, S. J., Letcher, R. A., and Croke, B. F. W.: Modelling floodplain inundation for environmental flows: Gwydir wetlands, Australia, Ecol. Model., 211, 350–362, 2008.
Risbey, J. S., Pook, M. J., McIntosh, P. C., Wheeler, M. C., and Hendon, H. H.: On the remote drivers of rainfall variability in Australia, Mon. Weather Rev., 137, 3233–3253, 2009.
Roshier, D. A., Whetton, P. H., Allan, R. J., and Robertson, A. I.: Distribution and persistence of temporary wetland habitats in arid Australia in relation to climate, Austral Ecol., 26, 371–384, 2001.
Schrier, G., Barichivich, J., Briffa, K. R., and Jones, P. D.: A scPDSI-based global data set of dry and wet spells for 1901–2009, J. Geophys. Res.-Atmos., 118, 4025–4048, 2013.
Shi, G., Ribbe, J., Cai, W., and Cowan, T.: An interpretation of Australian rainfall projections, Geophys. Res. Lett., 35, 1–6, 2008.
Skrzypek, G., Dogramaci, S., and Grierson, P. F.: Geochemical and hydrological processes controlling groundwater salinity of a large inland wetland of northwest Australia, Chem. Geol., 357, 164–177, 2013.
Slack, M., Fillios, M., and Fullagar, R.: Aboriginal settlement during the LGM at Brockman, Pilbara region, Western Australia, Archaeol. Ocean., 44, 32–39, 2009.
Sponseller, R. A., Heffernan, J. B., and Fisher, S. G.: On the multiple ecological roles of water in river networks, Ecosphere, 4, 17, 1–4, 2013.
Stendera, S., Adrian, R., Bonada, N., Cañedo-Argüelles, M., Hugueny, B., Januschke, K., Pletterbauer, F., and Hering, D.: Drivers and stressors of freshwater biodiversity patterns across different ecosystems and scales: a review, Hydrobiologia, 696, 1–28, 2012.
Taschetto, A. S. and England, M. H.: An analysis of late twentieth century trends in Australian rainfall, Int. J. Climatol., 29, 791–807, 2009.
Thomas, R. F., Kingsford, R. T., Lu, Y., and Hunter, S. J.: Landsat mapping of annual inundation (1979–2006) of the Macquarie Marshes in semi-arid Australia, Int. J. Remote Sens., 32, 4545–4569, 2011.
Trigg, M. A., Michaelides, K., Neal, J. C., and Bates, P. D.: Surface water connectivity dynamics of a large scale extreme flood, J. Hydrol., 505, 138–149, 2013.

Tweed, S., Leblanc, M., Cartwright, I., Favreau, G., and Leduc, C.: Arid zone groundwater recharge and salinisation processes; an example from the Lake Eyre Basin, Australia, J. Hydrol., 408, 257–275, 2011.
van Etten, E. J. B.: Inter-annual rainfall variability of arid Australia: greater than elsewhere?, Aust. Geogr., 40, 109–120, 2009.
Veenendaal, E. M., Ernst, W. H. O., and Modise, G. S.: Effect of seasonal rainfall pattern on seedling emergence and establishment of grasses in a savanna in south-eastern Botswana, J. Arid Environ., 32, 305–317, 1996.
Viles, H. A. and Goudie, A. S.: Interannual, decadal and multidecadal scale climatic variability and geomorphology, Earth-Sci. Rev., 61, 105–131, 2003.
Wang, L., Huang, R., and Wu, R.: Interdecadal variability in tropical cyclone frequency over the South China Sea and its association with the Indian Ocean sea surface temperature, Geophys. Res. Lett., 40, 768–771, 2013.
Wen, L., Macdonald, R., Morrison, T., Hameed, T., Saintilan, N., and Ling, J.: From hydrodynamic to hydrological modelling: investigating long-term hydrological regimes of key wetlands in the Macquarie Marshes, a semi-arid lowland floodplain in Australia, J. Hydrol., 500, 45–61, 2013.
Western Australia (WA) Department of Water: 708011: Foretescue River – Newman, River Monitoring Stations in Western Australia, available at: www.kumina.water.wa.gov.au/waterinformation/wir/reports/publish/708011/708011 (last access: 7 October 2014), 2014.
White, P. S. and Pickett, S. T. A. Natural disturbance and patch dynamics: an introduction, in: The Ecology of Natural Disturbance and Patch Dynamics, edited by: Pickett, S. T. A. and White, P. S. Academic Press, Orlando, USA, 3–16, 1985.
Xu, H.: Modification of normalised difference water index (NDWI) to enhance open water features in remotely sensed imagery, Int. J. Remote Sens., 27, 3025–3033, 2006.

Table 1. Model parameter estimates and standardized statistics for the final linear model to reconstruct historical flood area on the Fortescue Marsh, NW Australia.

Driver	β (km^2)	Effect	p value
R	144.729	+	< 0.001
R_d	−62.950	−	< 0.001
F_{At-1}	−29.157	±	< 0.001
Int	−7.650	−	0.070
Intercept	−8.040	−	0.816

Note: β = Weighted contribution; Effect = gain (+) or loss (−) effect of each variable on change in flood area (ΔF_A); R = total rainfall month^{-1} on the upper Fortescue catchment; R_d = number of days with > 0 mm rain month^{-1}; F_{At-1} = flood area of the previous month; Int = the time interval between observations; Intercept = equation intercept.

Table A1. Australian Bureau of Meteorology (BoM) rainfall stations (www.bom.gov.au/climate/data/) located within and nearby the upper Fortescue River catchment, NW Australia.

No	Station name	BoM number	Lat (° N)	Long (° E)	Status	Year open	Year closed
	Mulga Downs	5015	−22.10	118.47	Open	1898	
	Bulloo Downs	7019	−24.00	119.57	Open	1917	
	Marillana	5009	−22.63	119.41	Open	1936	
	Noreena Downs	4026	−22.29	120.18	Open	1911	
1	Balfour Downs	4003	−22.80	120.86	Closed	1907	1998
2	Wittenoom	5026	−22.24	118.34	Open	1949	
3	Auski Munjina Roadhouse	5093	−22.38	118.69	Open	1998	
4	Kerdiadary	5047	−22.25	119.10	Closed	1901	1910
5	Warrie	5025	−22.40	119.53	Closed	1927	1964
6	Bonney Downs	4006	−22.18	119.94	Open	1907	
7	Poondawindie	4063	−22.20	120.20	Closed	1930	1938
8	Sand Hill	5064	−22.78	119.62	Closed	1971	1984
9	Roy Hill	5023	−22.62	119.96	Closed	1900	1998
10	Ethel Creek	5003	−22.90	120.17	Closed	1907	2003
11	Packsaddle Camp	5089	−22.90	118.70	Closed	1989	2002
12	Rhodes Ridge	7169	−23.10	119.37	Open	1971	
13	Rpf 672 Mile	4065	−22.70	121.10	Closed	1913	1947
14	Billinnooka	13 029	−23.03	120.90	Closed	1960	1974
15	Jigalong	13 003	−23.36	120.78	Closed	1913	1991
16	Minderoo	7172	−23.40	119.78	Closed	1913	1931
17	Newman Aero	7176	−23.42	119.80	Open	1971	
18	Capricorn Roadhouse	7191	−23.45	119.80	Open	1975	
19	Murramunda	7102	−23.50	120.50	Closed	1915	1949
20	Sylvania	7079	−23.59	120.05	Open	1950	
21	Prairie Downs	7153	−23.55	119.15	Open	1968	
22	Turee Creek	7083	−23.62	118.66	Open	1920	
23	Mundiwindi	7062	−23.79	120.24	Closed	1915	1981
24	Rpf 561 Mile	13 013	−23.90	120.40	Closed	1913	1947
	Newman	7151	−23.37	119.73	Closed	1965	2003

Table A2. Climate variables used in the development of a linear model to reconstruct historical flood area on the Fortescue Marsh, NW Australia.

Interval	Variable	Res.	Location	Period	Source
d	*R*		Bulloo Downs	1917–2012	www.bom.gov.au/climate/data/
d	*R*		Marillana	1936–2012	www.bom.gov.au/climate/data/
d	*R*		Mulga Downs	1907–2012	www.bom.gov.au/climate/data/
d	*R*		Noreena Downs	1911–2012	www.bom.gov.au/climate/data/
m	*R*	1°	UF	1900–2012	www.bom.gov.au/cgi-bin/silo/cli_var/area_timeseries.pl
m	*R*	0.5°	UF	1901–2012	GPCC V6 rain gauge precipitation dataset
m	*R*	0.5°	UF	1901–2009	CRU time-series (TS) version 3.10.01 (land)
m	*T*	1°	UF	1910–2012	www.bom.gov.au/cgi-bin/silo/cli_var/area_timeseries.pl
m	*T*	0.5°	UF	1901–2009	CRU TS 3.10 (land)
m	PET	0.5°	UF	1901–2009	Schrier et al. (2013)

Note: Res. stands for the resolution of gridded data, d is daily weather station rainfall data, m is monthly gridded climate data, *R* is total rainfall (mm), *T* is mean temperature (°C) and PET is Penman–Monteith potential evapotranspiration index. UF is the upper Fortescue River catchment (31 000 km^2).

Table A3. Pearson correlation matrix of the variables included in the final linear model to reconstruct historical flood area on the Fortescue Marsh, NW Australia.

	R	R_d	F_{At-1}	Int
R	1	–	–	–
R_d	0.8518 $p < 0.001$	1	–	–
F_{At-1}	−0.0361 $p = 0.6507$	−0.0313 $p = 0.6943$	1	–
Int	0.0703 $p = 0.3767$	0.0089 $p = 0.9108$	−0.0162 $p = 0.8388$	1

Note: R = total rainfall month^{-1} on the upper Fortescue catchment (mm); R_d = number of days with > 0 mm rain month^{-1} (days); F_{At-1} = flood area of the previous month (km^2); Int = the time interval between observations (days).

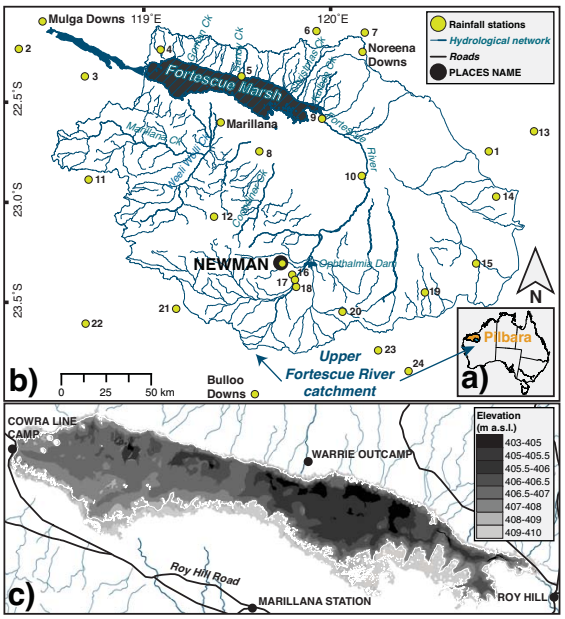

Figure 1. (a) The Pilbara region in northwest Australia, **(b)** upper Fortescue River catchment and river network (blue lines; WA Dept of Water, 2014), including the Fortescue Marsh's floodplain area used in this study (black hatched section; < 410 m a.s.l. extracted from a 1 s DEM-H, Geoscience Australia, 2011), and meteorological stations (green circles, see full list in Appendix A, Table A1; www.bom.gov.au/climate/data/) and **(c)** elevation of the study area (0.1 m vertical accuracy (RMS) LiDAR Survey DEM; Fortescue Metals Group Ltd, 2010) with roads and place name (black lines and circles; Geoscience Australia, 2001). *Generated in ArcMap v. 9.2.*

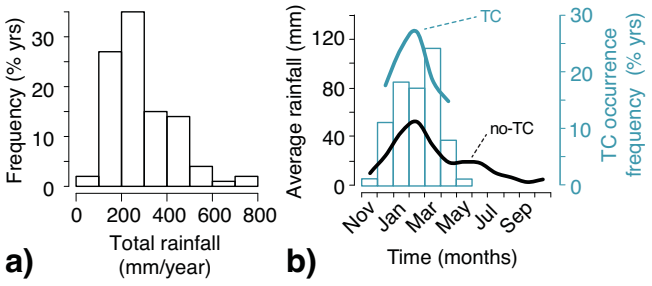

Figure 2. The upper Fortescue River catchment 1912–2012 hydroclimate with **(a)** frequency distribution of total yearly rainfall and **(b)** average monthly rainfall for months recording at least one tropical cyclone (TC) within 500 km radius of the upper Fortescue River catchment (blue line) and without TC recorded (black line), with the number of years (frequency) where TC occurrence was recorded for each month of the water year (blue columns); only one occurrence of TC was recorded in November and May for the last century and thus rainfall averages for these months were not included. Source: www.bom.gov.au/cgi-bin/silo/cli_var/area_timeseries.pl and www.bom.gov.au/cyclone/history/.

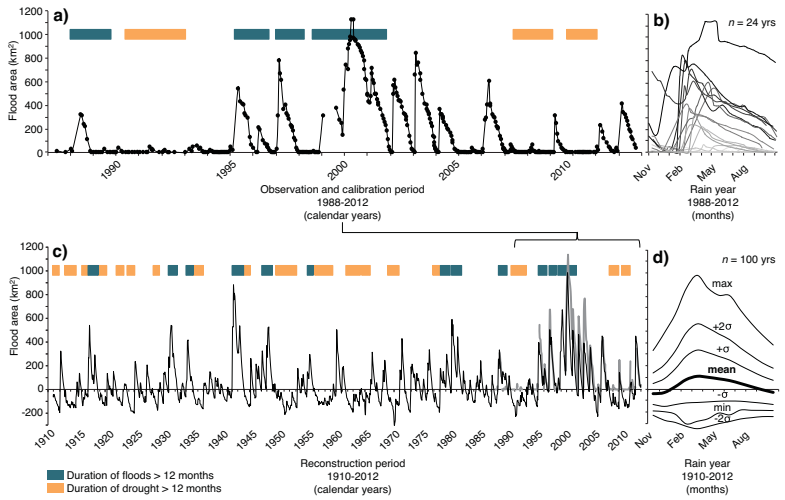

Figure 3. (a) 1988–2012 flood area observation and calibration dataset (solid black line with dots for each observation) and its **(b)** timing of seasonal change over the rain year (n = 24 yr); **(c)** 1912–2012 flood area reconstruction (solid black line) with the observation dataset plotted for the 1988–2012 period (solid grey line) for comparison and **(d)** monthly mean, minimum (min), maximum (max) and 1 and 2 σ ranges of variation over the rain year for the reconstructed period (n = 100 yr). Overlaid on **(a)** and **(c)** time-series are the supraseasonal dry and wet periods, where F_A was either < 0 or > 0 km^2 for over 12 consecutive months.

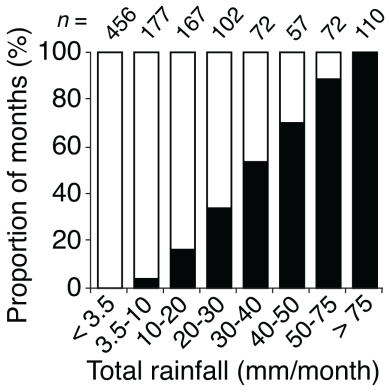

Figure 4. Total monthly rainfall in the upper Fortescue River catchment (total rainfall) causing an increase in surface water area measured as the proportion of months with net change in flood area or ΔF_A > 0 km^2 (black columns) at the Fortescue Marsh (1912–2012).

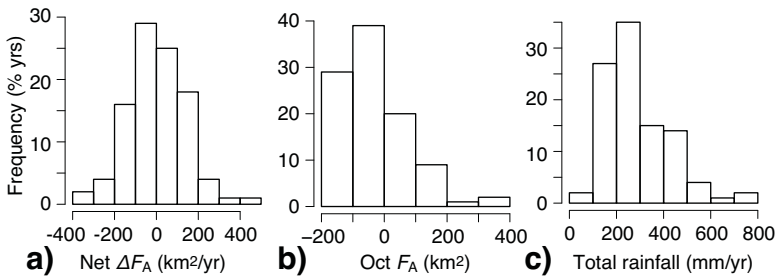

Figure 5. 1912–2012 frequency distributions of yearly **(a)** net change in flood area (ΔF_A), **(b)** end-of-the-year flood area (October F_A) and **(c)** yearly maximum flood area (F_{Amax}; km^2), n = 100 yr.

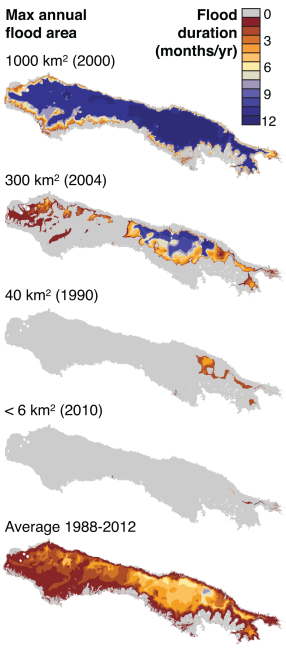

Figure 6. Maps of the Fortescue Marsh floodplain including flood duration isohyets over the rain year (November–October) representing examples of the main connectivity thresholds: wettest year observed in 2000 (F_{Amax} ~ 1000 km^2); a very large flood year in 2004 (F_{Amax} ~ 300 km^2); the long-term mean flood year in 1990 (F_{Amax} ~ 40 km^2) and a dry year in 2010 (F_{Amax} < 6 km^2) and the 1988–2012 average.

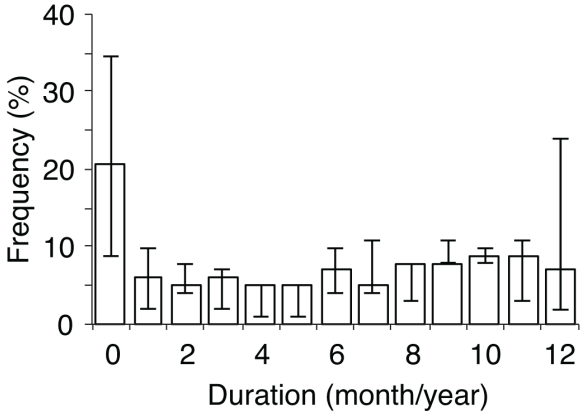

Figure 7. Frequency distribution of drought duration per annum (i.e., consecutive month with $F_A < 0\,km^2$), with error bars representing the variation in the distribution when threshold for drought duration is defined as $F_A < \pm 56\,km^2$ for the last century ($n = 100\,yr$).

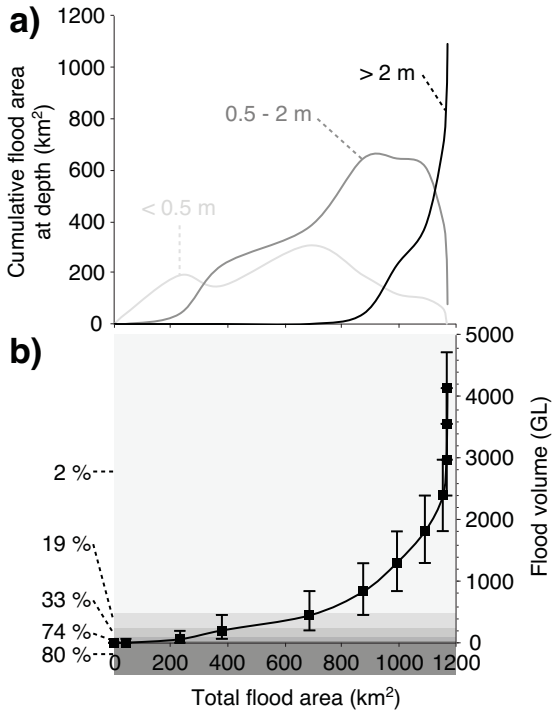

Figure 8. Total flood area at the Fortescue Marsh and **(a)** its proportion occupied by water depth shallower than 0.5 m (light grey), between 0.5 and 2 m (dark grey) and deeper than 2 m (black) and **(b)** the estimated volume of surface water (black line) with century frequencies (% yr) at which different thresholds (grey shading) were attained.

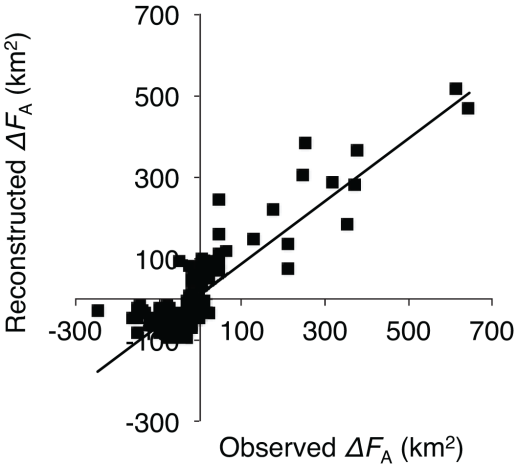

Figure A1. Observed against reconstructed monthly ΔF_A values (n = 160) for the 1988–2012 calibration period (R^2_{adj} = 0.79; p value < 0.001).